

Article

Degradation-resistant implanted biomaterials establish an immunosuppressive microenvironment that induces T cell exhaustion by recruiting myeloid cells

Qin Fan^{a,1}, Huaxing Dai^{a,1}, Jinyu Bai^{b,1}, Jialu Xu^a, Qingle Ma^a, Ziyang Fei^a, Xiaozhong Zhou^{b,*}, Kam W. Leong^{c,*}, Chao Wang^{a,*}

^a Institute of Functional Nano & Soft Materials, Jiangsu Key Laboratory for Carbon-based Functional Materials and Devices, Soochow University, Suzhou 215123, China

^b Department of Orthopedics, The Second Affiliated Hospital of Soochow University, Suzhou 215004, China

^c Department of Biomedical Engineering, Columbia University, New York, NY 10027, USA



ARTICLE INFO

Article history:

Received 5 July 2021

Received in revised form 30 August 2021

Accepted 13 October 2021

Available online 25 November 2021

Keywords:

TiO₂ nanoparticles

Immune microenvironment

Myeloid cells

Implants

Immunosuppressive

ABSTRACT

Implanted biomaterials have transformed healthcare and the treatment of injury and disease, but their influence on the local immune landscape remains unclear. Here we discovered that degradation-resistant titanium-based implants establish an immunosuppressive microenvironment by recruiting myeloid cells, including monocytes, macrophages, neutrophils, and myeloid-lineage dendritic cells. Unlike normal tissues, the tissues nearby implants exhibit a chronic inflamed and immunosuppressive status characterised by myeloid-rich, T cell-exhaustion gene signature by single-cell RNA sequencing. Vitamin C treatment provides an effective strategy to rescue the immunosuppressive microenvironment, which can be used as a regular supplement to reduce the risk of malignant cell survival around the implants.

1. Introduction

Implanted biomaterials are essential and ubiquitous in healthcare [1,2]. Tissue engineering, drug delivery, orthopaedic implants, immunotherapy, and many other medical fields rely on implantable biomaterials [3]. The immune system recognises non-self-implanted materials as foreign bodies, resulting in a dynamic immune microenvironment in the tissues surrounding implants [4,5]. Implanted biomaterials induce unwanted inflammation [6–9], which is the primary adverse reaction observed [10,11]. However, the extent to how implanted biomaterials shape the local immune landscape and impact clinical outcomes remains poorly understood.

In the current study, we discovered a phenomenon that foreign degradation-resistant implants can establish an immunosuppressive microenvironment by recruiting myeloid cells to induce T cell exhaustion, resulting in the promoted tumour growth at the injection site in multiple mice tumours models. In patients with orthopaedic steel plates (Ti alloy), we find that the surrounding tissue is infiltrated with CD11b⁺

myeloid cells coupled to the exhaustion status of T cells in the microenvironment. In mice, implanted TiO₂ nanoparticles (NPs) unintentionally establish an 'artificial' environment favouring tumour growth by recruiting immunosuppressive CD11b⁺ myeloid cells, resulting in T cell exhaustion and dysfunction at the local site. Vitamin C (ascorbic acid) is well-known for reducing the inflammatory response in patients and mice [12,13]. We demonstrate that vitamin C administration reshapes the immunosuppressive environments induced by the refractory-degradable implants via reprogramming immunosuppressive immune cells and alleviating T cell exhaustion.

2. Materials and Methods

2.1. Materials

TiO₂ (Macklin, catalogue no. T818936) was purchased from Shanghai Macklin Biochemical Co., Ltd. Single-walled carbon nanotubes (SWNTs; XFNANO, catalogue no. 101943) were purchased from Jiangsu Xianfeng Nanomaterials Technology Co., Ltd. Silicone gel was pur-

* Corresponding authors.

E-mail addresses: zhouxz@suda.edu.cn (X. Zhou), kam.leong@columbia.edu (K.W. Leong), cwang@suda.edu.cn (C. Wang).

¹ These authors contributed equally to this work.

chased from Shenzhen Hongyejie Technology Co., Ltd. Titanium alloy was purchased from Baoji Lifengyuan Titanium Co., Ltd. Ascorbate (Sigma-Aldrich, catalogue no. v900134-100g) was purchased from Suzhou Keqing Biological Reagent Co., Ltd. Penicillin-Streptomycin (Invitrogen, catalogue no. 15070063), DMEM/HIGH (Hyclone, catalogue no. SH30022.01), RPMI1640 (Hyclone, catalogue no. SH30809.01), and PBS (Hyclone, catalogue no. SH30256.01) were purchased from Suzhou Keyite Instrument Equipment Co., Ltd. Deionized water (18.2 MΩ.cm) was purchased from Million-Q.

2.2. Cell lines and mice

RAW 264.7 macrophages were purchased from the Shanghai Cell Bank of the Chinese Academy of Sciences. The RAW 264.7 cells were cultured in DMEM with higher glucose levels containing 10% fetal bovine serum and penicillin-streptomycin (100 U/mL). Mice B16F10 cells and lucifer-labelled B16F10 cells (B16F10-Luc) were gifts from Dr Wenjun Zhu of Suzhou University. B16F10-Luc cells were cultured using DMEM high-sugar medium containing 10% fetal bovine serum and penicillin-streptomycin (100 U/mL). Mice CT26 colon cancer cells were purchased from the American type culture collection. CT26 cells were cultured with RPMI 1640 medium containing 10% fetal bovine serum and penicillin-streptomycin (100 U/mL). C57BL/6J mice and BALB/c mice (6–8 weeks old) were purchased from Nanjing Pengsheng Biotechnology Co., Ltd. The breeding and mice experiments were carried out under the approval of Soochow University's animal ethics (Approval No. SUDA20210402A02).

2.3. Characterisation and modification of biomaterials

TiO₂ nanoparticles were prepared as a solution of 50 ng/mL using ultrasound to promote dissolution. The size of the TiO₂ nanoparticles was measured using a Malvern Nano Measurer. 7 μL samples were dried on a copper network by air drying and were photographed by transmission electron microscopy (TEM). The distribution of elements was determined by X-ray diffraction (XRD) analysis. TiO₂ NPs were injected into mice on days 1 and 7, removed for fixation and dehydration, and observed with a scanning electron microscope (SEM). To modify TiO₂ NPs, we used 4 mL dichloromethane (CH₂Cl₂) to dissolve TiO₂ NPs and DSPE-PEG at a ratio of 1:2, vacuum rotary evaporating for 15 min, and added water for an ultrasound to evenly disperse. Prepared samples were analysed using thermal analysers (TGA). The size of the TiO₂@DSPE-PEG NPs was measured with a Malvern Nano Measurer, and TEM was used to observe the nanostructure of the NPs.

2.4. Immune microenvironment surrounding titanium bone replacement implants in humans

Each patient's fixed steel plates were collected after surgery and rinsed with sterile neutral phosphate buffer, and the tissue remaining on the steel plate was collected. The patient's distal tissue was used as a control. The tissues were digested, and a single-cell suspension was prepared. The red blood cell lysate was used to eliminate interference caused by red blood cells in tissues. The cells were divided into several fractions and were stained with the following three sets of fluorescently-labelled antibodies: (1) FITC-CD45, PE-CD3, APC-PD-1; (2) FITC-CD11b, PE-CD14, and APC-PD-1; (3) FITC-CD11b, PE-CD15, and APC-PD-1; (4) FITC-CD11b, PE-CD11c, and APC-PD-1; (5) FITC-CD3, PE-LAG3 and CTLA-4; (6) (5) FITC-CD3, PE-TIM-3 and APC-PD1. Residual tissue was fixed with 4% polyformaldehyde, sliced for H&E staining and immunohistochemistry, and observed by microscopy. Cytokines (TNF-α, IL-1β, and IL-6) in tissues were extracted using tissue protein extraction reagents and were evaluated by ELISA. Human tissue analysis was approved by the Clinical Research Project of the Second Hospital affiliated with Suzhou University, which conformed to human ethics regulations (Approval No. JD-LK-2020-096-01).

2.5. Effect of TiO₂ nanoparticles on PD-1 expression in macrophages in vitro

RAW 264.7 cells were seeded in a 6-well plate at 3 × 10⁵ cells/well. After 6 h, 20 μg TiO₂ NPs were added to each well, and the cells were incubated for 24 h. 200 ng of lipopolysaccharide (LPS) was used as a control. RAW 264.7 cells were collected after treatment, cells were dyed with FITC-F4/80 and PE-PD-1, and PD-1 expression on the macrophage surface was analysed by flow cytometry. Western blot was used to analyse the macrophage expression of PD-1. Total amounts of proteins were measured with a BCA protein kit, and the protein content for each well was ~20 μg. The proteins were separated on a sodium thiamin sulfate-polyacrylamide gel and were transferred to a PVDF membrane. The membrane was incubated with primary anti-PD-1 and β-actin antibodies and with secondary antibodies. Chemical luminescent reagents were used for imaging.

Total RNA was extracted from RAW 264.7 cells using Trizol. The purity and concentration of total RNA were measured with a DS-11 series phosphor/fluorometer (Denovix). A First Chain cDNA Synthesis Kit was used to synthesise the first chain of cDNA by reverse transcription and amplify it by qPCR. The thermal cycler parameters were: 95°C, 10min; 95°C, 10s; 55°C, 1min; 45 cycles. The primer sequences were as follows: mouse PD-1 primers: forward primer 5'-GGTATCCCTGTATTGCTGCTGCTG-3' and reverse primer 5'-CTTCAGAGTGTGCTCCTTGCTTCC-3'; mouse TNF-α primers: forward primer 5'-ATGTCTCAGCCTCTTCATTC-3' and reverse primer 5'-GCTTGCTCACTCGAATTTTGAGA-3'; mouse IL-6 primers: forward primer 5'-CTCCCAACAGACCTGTCTATAC-3' and reverse primer 5'-CCATTGCACAACCTTTTCTCA-3'; mouse NF-κB primers: forward primer 5'-CAAAGACAAAGAGGAAGTGCAA-3' and reverse primer 5'-GATGGAATGTAATCCCACCGTA -3'; mouse β-actin primers (internal control): forward primer 5'-GTGCTATGTTGCTCTAGACTTCG-3' and reverse primer 5'-ATGCCACAGGATCCATACC-3'. Gene expression levels were calculated using the ratio = 2^{-ΔΔCT} method.

To measure PD-1 expression on macrophages more intuitively, we inoculated RAW 264.7 cells on slides, added TiO₂ NPs as described above, and stained them with FITC-F4/80, PE-PD-1 for 1 h. Polyformaldehyde was used to fix cells for 30 min. The nucleus was stained with DAPI. Samples were sealed with Fluoromount Aqueous Mounting Medium then were observed by confocal microscopy.

We used inhibitors to block the NF-κB pathway to analyse the correlation between the NF-κB signalling and PD-1 expression stimulated by TiO₂ NPs. RAW 264.7 cells (3 × 10⁵) were seeded in a 6-well plate. Bay (10 μM) and CIL inhibitors (2 μM) were added, and the cells were cultured for 1 h. Then, 20 μg of TiO₂ NPs were added, incubating the cells for another 24 h. The cells were collected for flow cytometry and qPCR analysis of PD-1 expression.

2.6. Analysis of immune microenvironment surrounding TiO₂ NP injection site

C57BL/6J mice were divided randomly into two groups of 3–4 mice. 5 mg of TiO₂ NPs was injected into the back of mice subcutaneously on days 0 and 3, and the TiO₂ NPs and adjacent tissues were removed. Tissues from untreated mice were named the UNTX group. Half of the tissue was digested to prepare a single-cell suspension. The single-cell suspension was centrifuged at 1,800 rpm, the supernatant was removed, red blood cell lysate was added and allowed to react for 5 min, and the cells were washed three times with FACS buffer. The collected cells were divided into six groups for staining: (1) FITC-CD45, PE-CD3, and APC-PD-1; (2) FITC-CD11b, PE-CD14, and APC-PD-1; (3) FITC-CD11b, PE-Gr-1, and APC-PD-1; (4) FITC-CD11b, PE-CD11c, and APC-PD-1; (5) FITC-CD3, APC-CTLA-4, and PE-TIM-3; (6) FITC-CD3 and PE-LAG-3. The other half of the tissues and the main organs of the mice were fixed with 4% paraformaldehyde and were sectioned. H&E staining and immunohistochemical staining (PD-1, CD3, and F4/80) were performed

by Wuhan Service Biotechnology Co., Ltd. 5 mg of TiO₂ NPs were injected into the mice's back described above, and blood and serum were collected for routine blood analysis and blood biochemical analysis. Cytokines in the tissues surrounding the injection site were extracted using a tissue protein extraction reagent and were tested with a mouse multi-cytokine panel.

2.7. Single-cell transcriptomic analysis of immune microenvironment induced by TiO₂ NP injection

5 mg of TiO₂ NPs was injected into the back of the mice. Three days later, formed TiO₂ niches (without adjacent tissues) were removed and digested into a single-cell suspension. The cells were adjusted to a concentration of 700–1,200 cells/L. Gel beads containing barcode information were allowed to bind to a mixture of cells and enzymes and were enveloped in oil surfactant droplets in a microflow "double-cross" system to form gel beads-in-emulsions (GEMs). GEMs flowed into the reservoir and were collected, and the gel beads interpreted the barcode sequence, reversed the transcription of cDNA fragments, and marked the samples. Gel beads and oil droplets were broken, and PCR amplification was performed using cDNA as a template. All GEM products were mixed to build a standard sequencing library. High-volume sequencing of the library was performed using the two-end sequencing mode of an Illumina sequencing platform.

2.8. Anti-PD-1 antibody mouse treatment

The 6-8-week-old C57BL/6J mice were divided randomly into four groups: IgG, aPD-1, TiO₂+IgG, and TiO₂+aPD-1. Mice in the TiO₂+IgG and TiO₂+aPD-1 group were injected into the right-back of the mice with 5 mg TiO₂ on day 0. For the IgG and anti-PD-1 groups, the same volume of PBS was injected subcutaneously. B16F10 tumour cells (1×10^6) were injected near the TiO₂ NP injection site on day 2. For anti-PD-1 treatment, tumour-bearing mice were treated intravenously with 50 μ g anti-PD-1 monoclonal antibody in 200 μ L PBS on days 3, 4, and 5. The same dose of rat IgG was given to control mice.

2.9. Effects of TiO₂ nanoparticles on tumour growth

To study the effect of TiO₂ nanoparticles on tumour growth, we divided C57BL/6J mice into two groups of 5-6 mice. After mice were anaesthetised with 2.5% isoflurane, 5 mg of TiO₂ NPs were injected subcutaneously on the mice's left side. Melanoma cells (B16F10-Luc) and CT26 tumour cells were digested with trypsin and washed three times with sterile PBS. 50 μ L of B16F10 tumour cells (1×10^6 cells per mouse) were injected near the TiO₂ NP injection site. Tumour growth in mice was monitored. To study the effects of other biomaterials on tumour growth, silicone gel (250 μ g/mice), SWNT (0.3 mg/mice), titanium alloys (0.4 g/mice), and polyimide (0.002 g/mice) were injected or implanted into mice in a similar manner. Melanoma B16F10 cells were injected at sites adjacent to the biomaterial injection sites. SWNT and silicone gel groups, Ti alloy and PI groups shared the same control group, respectively. We synthesised PEGylated TiO₂ NPs (TiO₂@DSPE-PEG) to observe the effect of this modification on tumour growth. C57BL/6J mice were divided randomly into 5-6 mice: PBS, TiO₂ NP, and TiO₂@DSPE-PEG. 5 mg TiO₂ NPs and the same dose of TiO₂@DSPE-PEG NPs were injected subcutaneously, then 1×10^6 B16F10 cells were injected nearby. Tumour growth was measured every two days using an electronic digital calliper. Tumour volumes were calculated as $V = \text{short diameter}^2 \times \text{long diameter} \times 0.5$.

2.10. Effect of vitamin C on PD-1 expression in macrophages following TiO₂ NP intervention

RAW 264.7 cells (3×10^5) were seeded in a 6-well plate. The four experimental groups were control, LPS (200 ng), TiO₂ NP (20 μ g), and

TiO₂ NP plus vitamin C (20 μ g TiO₂ NP and 10 μ g vitamin C). The cells were cultured with treatments for 24 h then were collected for analysis. To measure the expression of PD-1, macrophages were stained with FITC-F4/80 and PE-PD-1 and were analysed by flow cytometry. The expression of PD-1, NF- κ B, IL-6, and TNF- α mRNA was analysed by qPCR.

2.11. Effect of vitamin C on immunosuppressive microenvironment induced by TiO₂ NP injection

C57BL/6J mice were divided randomly into two groups after being weighed. 5 mg of TiO₂ NPs was injected subcutaneously on day 0. Vitamin C was administered intraperitoneally on days 0 and 2 at a dosage of 4 g/kg. Mice were euthanised on day 3. The TiO₂ NPs and adjacent tissue were collected and digested for flow cytometric analysis into a single cell suspension. The cells were stained with the following sets of fluorescently-labelled antibodies: (1) FITC-CD3, APC-CD8, PerCP-CD4, PE-PD-1; (2) FITC-CD3, APC-CD8, PE-TIM3; (3) FITC-CD3, APC-CD8, PE-LAG3; (4) FITC-CD3, APC-CD8 and PE-CTLA-4; (5) FITC-CD11b, PE-Ly6G, APC-PD-1; (6) PE-CD45, FITC-CD11b, APC-Gr-1; (7) FITC-CD11c, APC-PD-1; (8) FITC-F4/80, APC-PD-1.

To study the effect of vitamin C on tumour growth, C57BL/6J mice were weighed and divided randomly into three groups. 5 mg of TiO₂ NPs was injected, or 200 μ L silicone gel was implanted subcutaneously in the back at day 0. TiO₂ and silicone gel experiments shared the same control group. Then, B16F10-Luc cells (1×10^6) were injected near the TiO₂ injection site. Vitamin C was administered intraperitoneally on days 0, 2, 4, 6, and 8 at a 4 g/kg dosage. Tumour sizes and mouse weights were measured every two days. Tumour volume was calculated as described above. The growth of the B16F10-Luc tumour in C57BL/6 mice was monitored every five days using an IVIS Spectrum Imaging System (PerkinElmer Ltd.). 15 mg/kg of fluorescent substrates (D-luciferin, potassium salt) was injected intraperitoneally. After 10 min, mouse bioluminescence was imaged using an exposure of 2 min. IVIS Living Image 4.2 software was used to quantify the bioluminescence signals. On day 15, mice were sacrificed, and tumours were harvested from mice for immunological evaluation. The prepared single-cell suspension was stained with FITC-CD3 and PE-CD8 antibodies.

3. Results

3.1. Titanium bone replacements recruit CD11b⁺ myeloid cells and cause elevated PD-1 expression in human patients

Degradation-resistant titanium-based materials have been used for decades in clinical applications, such as bone replacement, but their effects on the local immune microenvironment remain unclear. To investigate changes in the tissue microenvironment, samples from residual tissues on steel plates removed from human patients and normal tissues were collected and analysed through immunohistochemical staining and flow cytometry. Unlike normal tissues, tissues surrounding titanium plates were suffused with CD11b⁺ myeloid cells, such as monocytes/macrophages, neutrophils, and myeloid-lineage dendritic cells (DCs) (Fig. 1a-f). Expression of programmed cell death-1 (PD-1), a negative regulator of T cell development and a hallmark of T cell exhaustion, was greater in T cells from tissue around implants than in normal tissue (Fig. 1g-i). Other T cell dysfunction markers, including T-cell immunoglobulin mucin-3 (TIM-3), lymphocyte activation gene 3 protein (LAG-3), and cytotoxic T lymphocyte-associated antigen-4 (CTLA-4), were also up-regulated in tissues near orthopaedic implants (Fig. S1a). PD-1 expression was also elevated in monocytes/macrophages, neutrophils, and myeloid-lineage DCs (Fig. 1j-q). Levels of the inflammatory cytokines TNF- α , interleukin-1 β (IL-1 β), and interleukin-6 (IL-6) were also higher in tissues surrounding implants than in normal tissue (Fig. 1r-t).

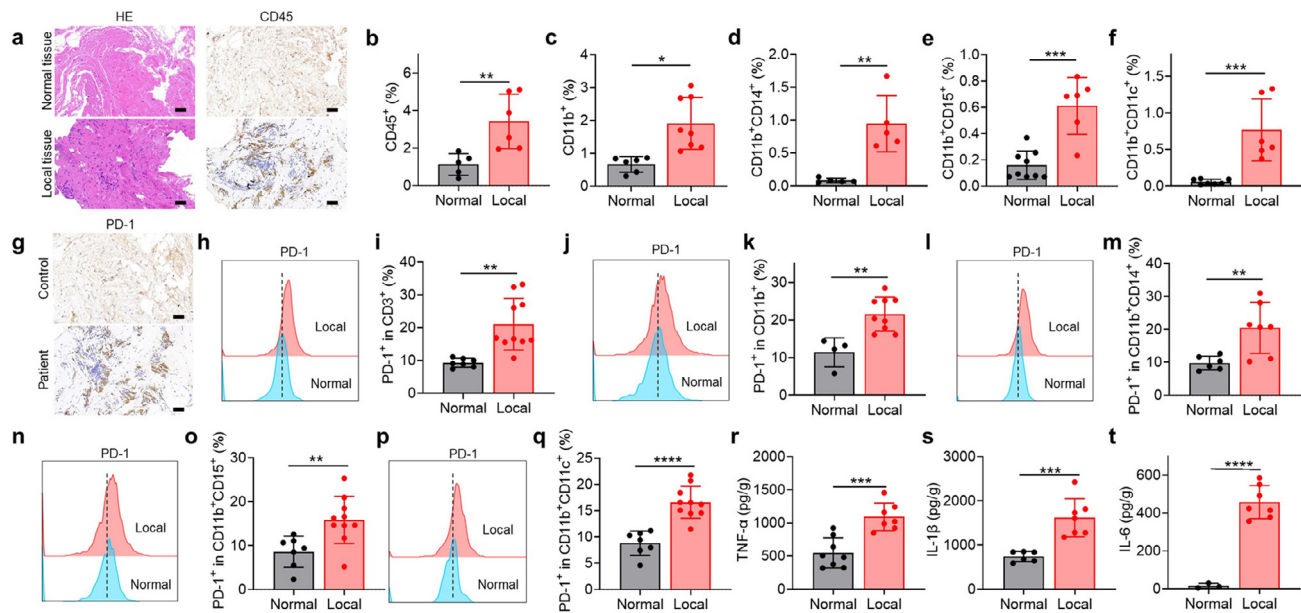


Fig. 1. Tissues adjacent to orthopedic implants in humans exhibit an exhausted T cell phenotype. (a) H&E staining and CD45 immunohistochemistry analysis of tissues adjacent to orthopedic implants. Scale bar, 50 μm . (b–f) Proportions of various immune cells in tissues (“local” means tissue adjacent to an implant) based on flow cytometry: (b) leukocytes (CD45⁺), (c) myeloid cells (CD11b⁺), (d) monocytes/macrophages (CD11b⁺CD14⁺), (e) neutrophils (CD11b⁺CD15⁺), (f) dendritic cells (CD11b⁺CD11c⁺). (g) Immunohistochemistry analysis of PD-1 expression. (h–q) Flow cytometry images and corresponding quantitation of PD-1 expression in (h, i) T cells, (j, k) myeloid cells, (l, m) monocytes/macrophages, (n, o) neutrophils, and (p, q) DCs. (r–t) Concentrations of the inflammatory cytokines TNF- α (r), IL-1 β (s), and IL-6 (t). Data are mean \pm SEM (n=6–10). * P <0.05, ** P <0.01, *** P <0.005, **** P <0.001 by Student’s t -test.

3.2. TiO₂ nanoparticles injected in mice recruit CD11b⁺ myeloid cells and induce T cell exhaustion

A titanium oxide layer on titanium materials is essential for maintaining bone integration and preventing corrosion [14,15]. Nevertheless, some corrosion of titanium materials in the body does occur and releases many titanium oxide nanoparticles [16,17]. To investigate the effect of such particles on the tissue microenvironment, we injected titanium dioxide nanoparticles subcutaneously into mice. Mice were injected with 5 mg of sterile TiO₂ NPs, and adjacent tissues were collected after 3 days for analysis and comparison with the tissue from untreated mice. A greater abundance of immune cells was observed at the injection site than untreated mice (Fig. 2a). Mice injected with TiO₂ NPs showed a ~6.2-fold increase in CD45⁺ leukocytes at the injected site relative to tissue from untreated mice (Fig. 2b). Similar to clinical samples, abundant CD11b⁺ myeloid cells (including monocytes/macrophages, myeloid-lineage DCs, and myeloid-derived suppressor cells (MDSCs)) were observed near the tissue of mice injected with TiO₂ NPs, (Fig. 2c–f). Analysis of the two major subtypes of MDSCs [18] revealed that the increase of monocytic MDSCs was more evident than granulocytic MDSCs (Fig. S2c and d). A significant increase in white blood cells and myeloid cells in the peripheral blood of mice treated with TiO₂ NPs was observed compared to the control mice (Fig. 2g). However, the expression of PD-1 was increased on the infiltrating immune cells but not on circulating immune cells (Figs. 2h–n, S1b–g, and S2a). Myeloid cells could suppress T cell function through multiple mechanisms [19–21]. Interaction of the PD-L1/PD-1 negatively regulates cytokine production and proliferation of T cells [22]. T cell exhaustion was further confirmed by the elevation of PD-1 and TIM-3 double-positive T cells (Fig. 2o–q, Fig. S2b). In addition, the immunosuppressive cytokine IL-10 was significantly higher than that of the control group (Fig. S2e). Together, these results indicated that TiO₂ NP injection caused a rapid influx of myeloid cells, leading to immunosuppressed T cells and inflammatory cytokine production. Meanwhile, blood routine analysis showed no significant changes in red blood cell and platelet counts or haemoglobin levels (Fig. S3a–j), and blood biochemical indexes remained unchanged, including levels of uric

acid, aspartate transaminase, alanine aminotransferase, and creatinine (Fig. S3k), indicating no significant toxicity to the main organs (heart, liver, spleen, lung, and kidney) (Fig. S4a). The results suggested that the injected TiO₂ NPs reshaped the local immune microenvironment by recruiting myeloid cells, but did not have a systematic effect.

We determined the mechanism by which the injected TiO₂ NPs induced PD-1 expression. Macrophage is an essential CD11b⁺ myeloid cell that participates in the body’s immune response to foreign implants. We investigated the effects of TiO₂ NPs on macrophages *in vitro*. RAW 264.7 cells were cultured with sterile TiO₂ NPs for 24 h. Confocal microscopy showed that PD-1 signals on the macrophage membrane were stronger on TiO₂ NP-treated cells than on untreated cells (Fig. 2r). This result was confirmed by flow cytometry data, western blot and RT-PCR analyses (Fig. 2s–v). PD-1 gene expression was approximately 3.3-fold higher in TiO₂ NP-treated cells than in untreated cells (Fig. 2v). NF- κ B regulates PD-1 expression in macrophages [23]. To verify that the increased PD-1 expression depended on the NF- κ B pathway, we used the NF- κ B inhibitor BAY 11-7082 to inhibit phosphorylation and degradation of I κ B α and subsequent nuclear transport of NF- κ B. BAY 11-7082 treatment significantly reduced the upregulation of PD-1 caused by TiO₂ NP treatment (Fig. 2w–y). This effect was blocked by the TLR4 inhibitor Resatorvid (Fig. 2z), demonstrating that the enhanced expression of PD-1 in macrophages depended on TLR4-NF- κ B signalling. In addition, we studied the *in vitro* effect of TiO₂ NPs on the PD-1 expression of T cells. However, the markers on the surface of T cells did not change significantly during the 24-hour incubation period (Fig. S4), implying that activated myeloid-derived cells may play an essential role in the stimulation of PD-1 expression on the surface of T cells.

3.3. TiO₂ implants alter the local immune microenvironment

To further characterise changes in the immune microenvironment induced by injection of TiO₂ NPs, we performed single-cell RNA sequencing (scRNA-seq) [24] with a 10X Genomics Chromium system. The tissues were digested into a single cell suspension for analysis. Nine main cell clusters were identified, including monocytes (26.8% of

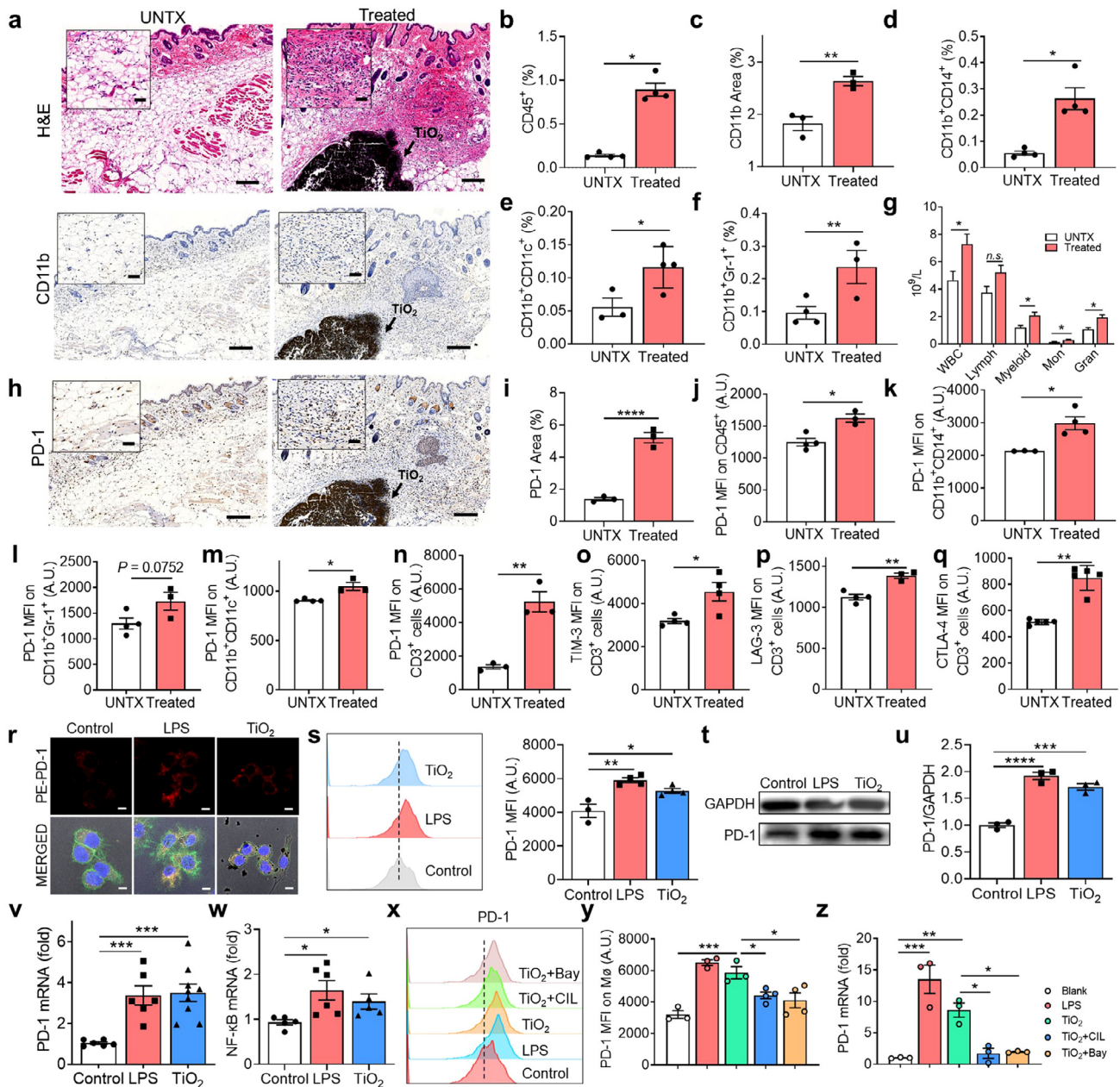


Fig. 2. TiO_2 implants induce T cell exhaustion by recruiting immunosuppressive immune cells. (a) Immunohistochemical analysis of tissues surrounding injected TiO_2 nanoparticles (NPs) on day 3. Scale bar, 100 μm . "UNTXX" indicates untreated control. (b) The proportion of leukocytes (CD45^+) in tissues surrounding injected TiO_2 NPs on day 3. (c) CD11b expression based on immunohistochemistry analysis. (d) Proportion of monocytes/macrophages ($\text{CD11b}^+\text{CD14}^+$), (e) DCs ($\text{CD11b}^+\text{CD11c}^+$), and (f) myeloid-derived suppressor cells ($\text{CD11b}^+\text{Gr-1}^+$) in tissue surrounding injected TiO_2 NPs based on by flow cytometry. (g) Blood routine analysis for mice with and without TiO_2 NP injection. (h) Immunohistochemical analysis of PD-1 expression in tissues on day 1 (scale bar, 100 μm) and (i) corresponding quantitation. (j–m) TiO_2 NP-induced PD-1 expression in (j) leukocytes, (k) monocytes/macrophages, (l) MDSCs, and (m) DCs. (n–q) Analysis of PD-1 (n) and the T cell exhaustion markers TIM-3 (o), LAG-3 (p) and CTLA-4 (q) in CD3^+ T cells after TiO_2 NP treatment. (r) Confocal image of PD-1 expression on macrophages. (s) Flow cytometry image and quantitative analysis of PD-1 on RAW 264.7 cells after co-culture with TiO_2 NPs. (t) Western blot analysis of PD-1 expression in RAW 264.7 cells (GAPDH was used as the reference), and (u) corresponding quantitation of PD-1. (v) PCR analysis of PD-1 mRNA expression. (w) NF- κB mRNA expression by RAW 264.7 cells. (x) Flow cytometry chart of PD-1, and (y) quantitation of PD-1. (z) PCR analysis of PD-1 mRNA expression on RAW 264.7 cells after different treatments. Values indicate mean \pm SEM ($n=3-6$). * $P<0.05$, ** $P<0.01$, *** $P<0.005$, **** $P<0.001$ by Student's *t*-test and one-way ANOVA using the Tukey post-test.

the total cells), macrophages (21.9%), fibroblasts (28.4%), neutrophils (6.7%), natural killer cells (7.3%), DCs (3.2%), T cells (3.1%), endothelial cells (1.9%), and satellite cells (0.6%) (Fig. 3a, b and Fig. S5a), indicating significant infiltration of the tissue by a variety of immune cells. The immune cell phenotypes in implant and normal tissues were analysed in detail. Analysis of the top 50 differentially expressed genes indicated that monocytes and macrophages in TiO_2 NP-injected tissue underwent significant transcriptomic changes (Fig. 3c).

TiO_2 NP injection-induced activation of inflammatory responses in recruited mononuclear phagocytes (Fig. 3d). NF- κB transcription factor activity was increased in monocytes and macrophages accumulated at the injection site, indicated by up-regulation of the NF- κB -related genes *Nckap11*, *Cyfp1*, *Flna*, *Pycard*, *Ikbke*, and *Arhgd1bm* (Fig. S5c). Expression levels of genes associated with immune suppression by macrophages (*Nfe2l2*, *Acod1*, *Il1b*, *Cybb*, *Trem1*, and *Trem2*) also increased (Fig. 3e). In addition, the *Nlrp3* gene was activated as well [25–27], indicat-

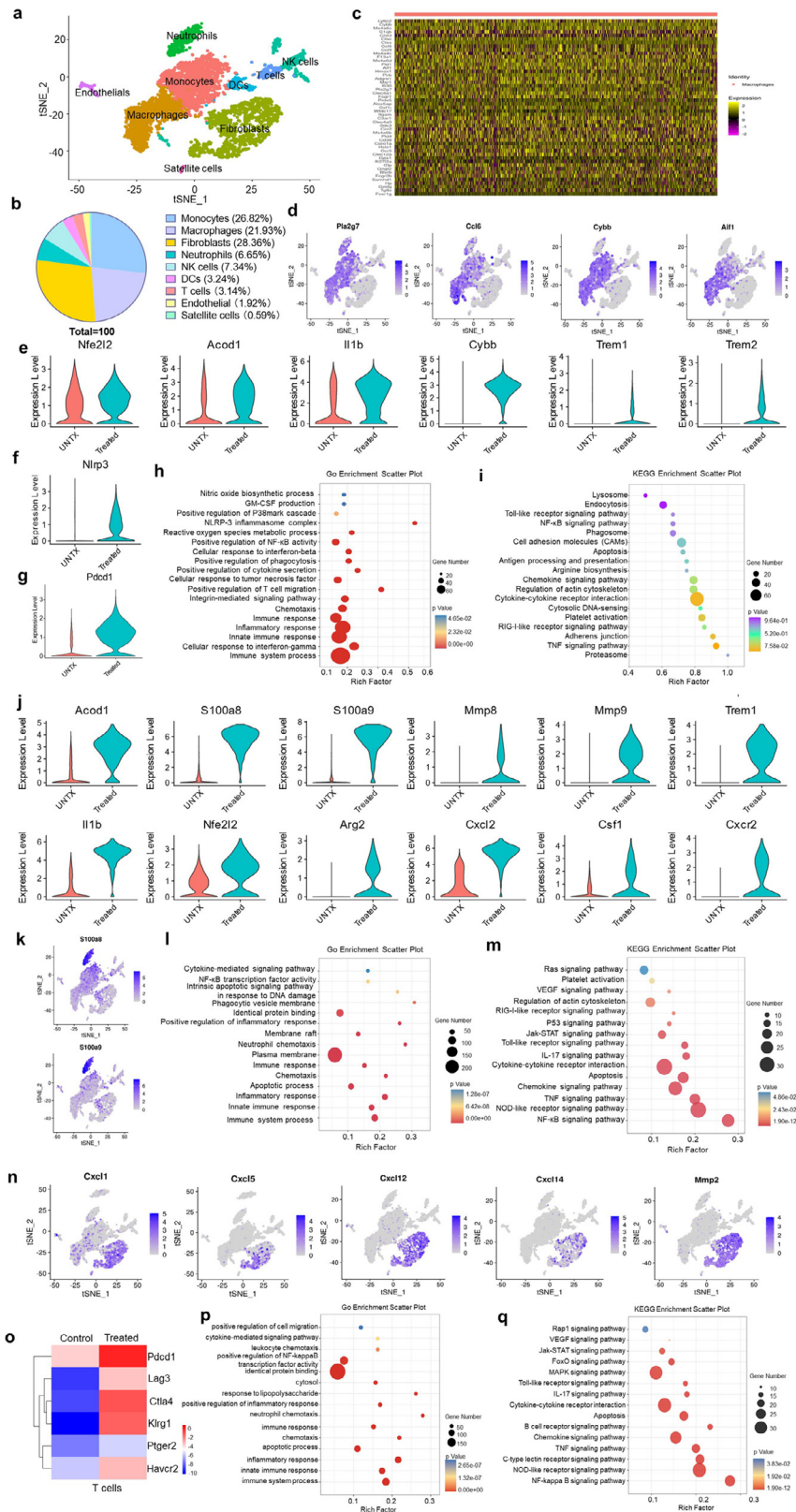


Fig. 3. Injected TiO₂ nanoparticles alter the local immune microenvironment. (a) t-stochastic neighbour embedding (t-SNE) visualisation of FACS of cells collected from mice with and without injection of TiO₂ NPs. (b) Cell composition of the tissue surrounding the injection site. (c) Heatmap of the top 50 differentially expressed genes in macrophages. (d) t-SNE map of 4 differential inflammatory marker genes in the mononuclear phagocyte system. (e) Expression levels of genes associated with immune suppression in macrophages. (f and g) Violin plots of expression of *Nlrp3* (f) and *Pdcd1* (g) in macrophages. (h) GO enrichment scatterplot and (i) KEGG enrichment scatterplot of macrophages. (j) Violin plots showing differentially expressed genes associated with immune suppression in neutrophils. (k) t-SNE map of *S100a8* and *S100a9* gene expression. (l) GO enrichment scatterplot and (m) KEGG enrichment scatterplot in neutrophils. (n) t-SNE map of differential expression of marker genes in fibroblasts. (o) Heat map of the differentially expressed genes associated with T cell exhaustion. (p) GO enrichment scatterplot and (q) KEGG enrichment scatterplot in neutrophils (n=3).

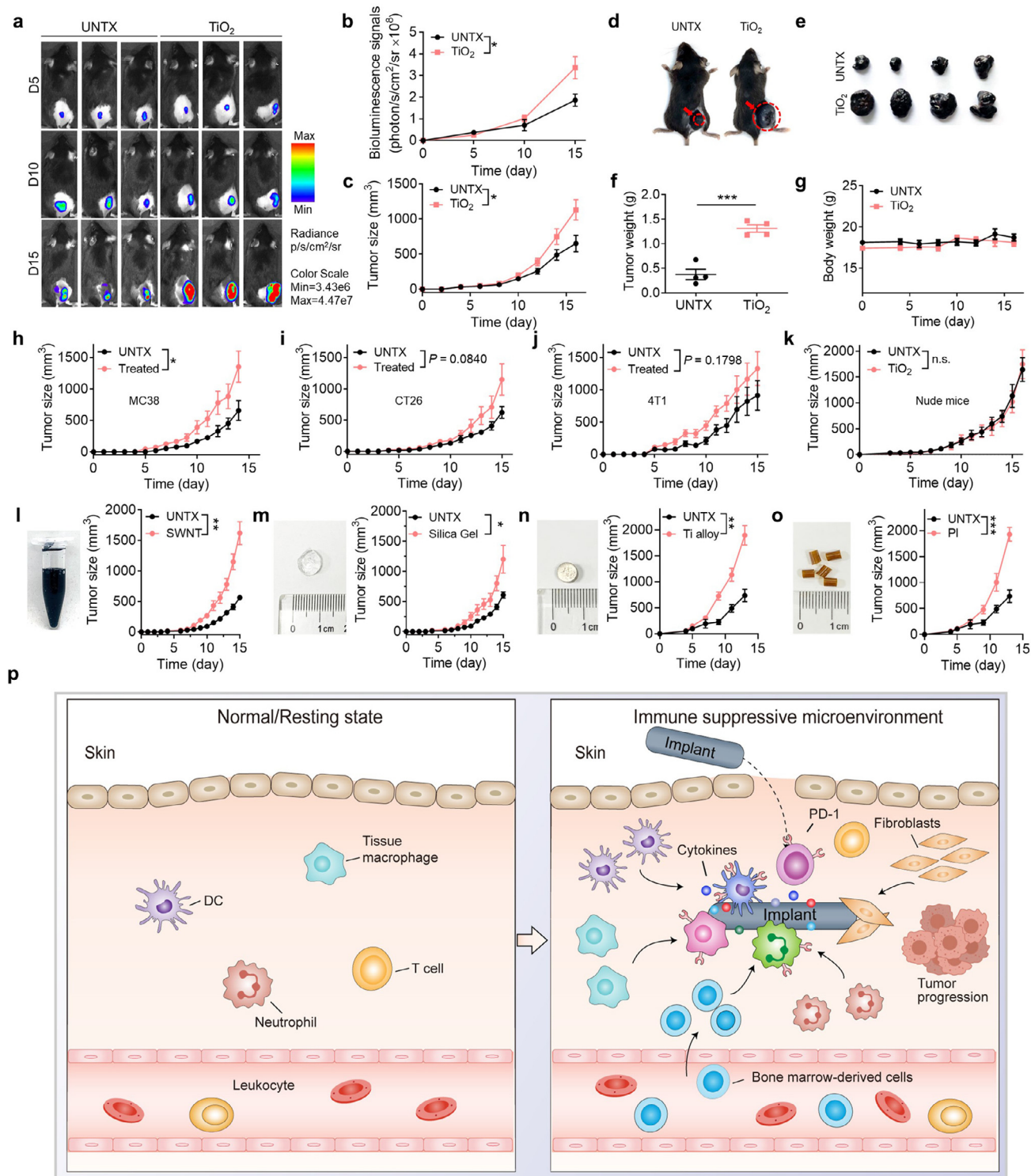


Fig. 4. Injected TiO₂ nanoparticles promote tumour growth in mice. (a) Bioluminescence images of B16F10-Luc tumour in mice with or without TiO₂ injection (UNTX, untreated control), and (b) quantitation of average luminescence intensity. (c) Average tumour growth and (d) photograph of tumour-bearing mice in different treatment groups. (e) Photograph of tumours and (f) weight of B16F10-Luc tumour removed on day 16 from mice injected with TiO₂ NPs. (g) Bodyweight of mice after TiO₂ NP injection. (h-j) Average tumour growth in mice using different tumour models: (h) MC38, (i) CT26, and (j) 4T1 carcinoma tumour model. (k) Average tumour growth curve of B16F10 tumour in nude mice with or without TiO₂ NP injection. (l-o) Left: photographs of (l) single-walled carbon nanotube (SWNT) suspension, (m) silica gel, (n) titanium alloy, and (o) polyimide; right: average tumour growth curve of mice injected with (l) SWNT suspension, (m) silica gel, (n) titanium alloy, and (o) polyimide. (p) A schematic diagram of refractory-degradable implanted biomaterials establishes an immunosuppressive microenvironment. Values indicate mean ± SEM (n=4-5). **P*<0.05, ***P*<0.01, ****P*<0.005 by Student's *t*-test.

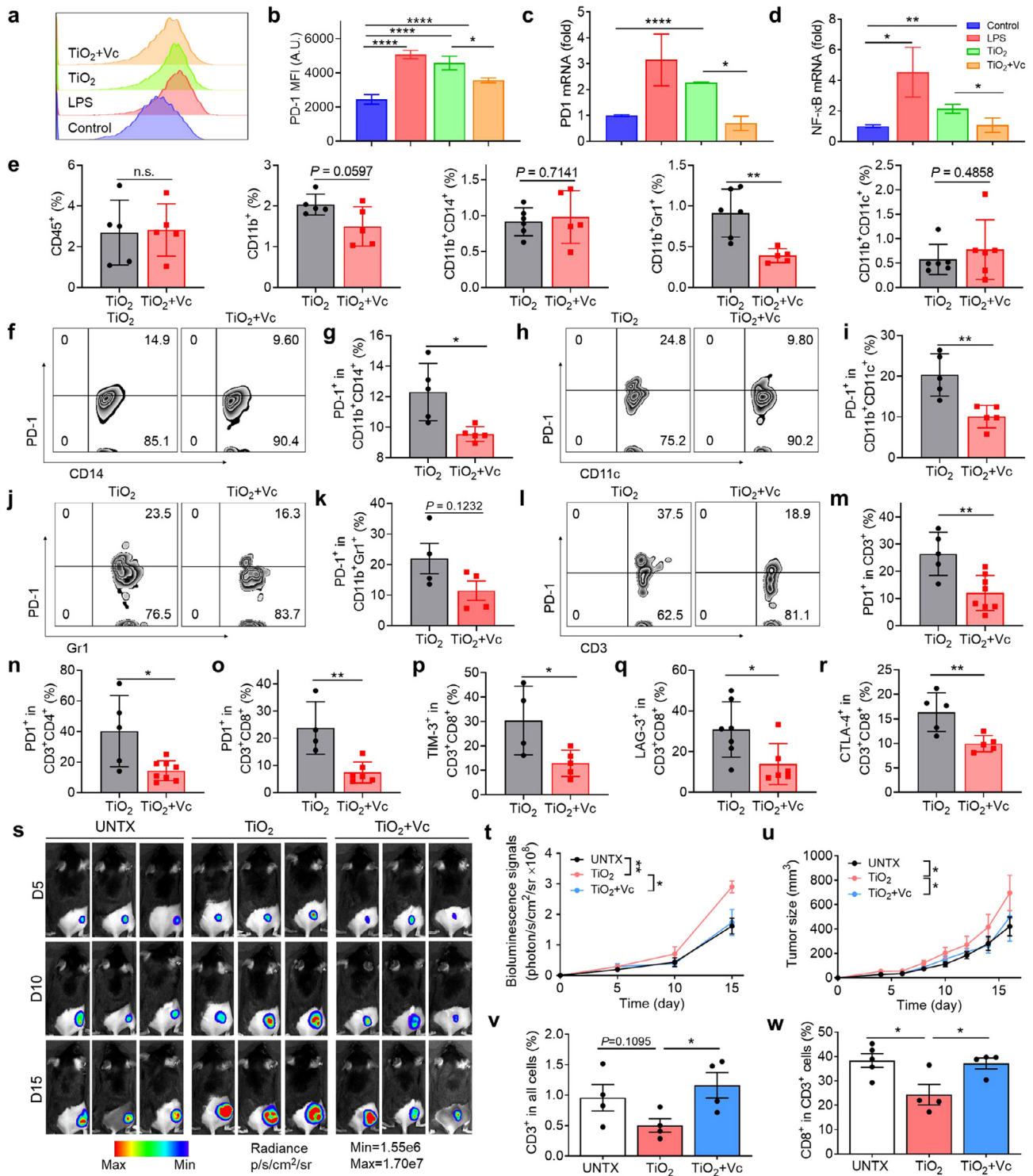


Fig. 5. Vitamin C abolishes the immunosuppressive microenvironment induced by TiO₂ nanoparticles. (a) Flow cytometry chart of PD-1 and (b) quantitation of PD-1 in RAW 264.7 cells after treatments. (c) PCR analysis of PD-1 mRNA and (d) NF- κ B mRNA expression. (e) Proportion of immune cells in tissues after vitamin C treatment, including leukocytes (CD45⁺), myeloid cells (CD11b⁺), monocytes/macrophages (CD11b⁺CD14⁺), MDSC (CD11b⁺Gr1⁺), and dendritic cells (CD11b⁺CD11c⁺). (f) Flow cytometry analysis and (g) quantitation of PD-1 in monocytes/macrophages in the tissue after vitamin C treatment. (h) Flow cytometry image and (i) quantitation of PD-1⁺ DCs. (j) Flow cytometry image and (k) of PD-1⁺ MDSCs. (l) Flow cytometry image and (m) quantitative analysis of PD-1⁺ T cells. (n) The proportion of PD-1 expression on CD3⁺CD4⁺ and (o) CD3⁺CD8⁺. (p) The proportion of TIM-3 expression on CD3⁺CD8⁺ T cells. (q) Quantitative analysis of LAG-3 expression on CD3⁺CD8⁺ T cells and (r) CTLA-4 expression on CD3⁺CD8⁺ T cells. (s) Representative bioluminescence images of the B16F10-Luc tumour after Vit C treatment and (t) average radiance of tumours in mice. (u) The average tumour growth curves of mice receiving the indicated treatments. (v) The percent of CD3⁺ cells in the tumour and (w) the proportion of the CD8⁺ in CD3⁺ cells in the tumour. Values indicate mean \pm SEM (n = 4–8). **P*<0.05, ***P*<0.01, ****P*<0.005, *****P*<0.001 by Student's *t*-test and one-way ANOVA using the Tukey post-test.

ing inflammation-associated pathological changes at the injection site (Fig. 3f). TiO₂ NP-treated macrophages showed greater PD-1 expression than untreated cells (Fig. 3g), as observed previously. Based on GO and KEGG enrichment analysis, multiple signalling pathways for macrophage-related immune suppression were activated in tissues surrounding TiO₂ NPs, including pathways responsible for inflammation, NF- κ B activation, production of nitric oxide, and the inflammasome (Fig. 3h, i).

Neutrophils facilitate tumour metastasis by damping anti-tumour immunity [28]. TiO₂ NP injection caused significant changes in neutrophil gene expression (Fig. S5d). Violin plots showed genes associated with immune suppression (*Acod1*, *S100a8*, *S100a9*, *Mmp8*, *Mmp9*, *Trem1*, *Il1b*, *Nfe212*, *Arg2*, *Cxcl2*, *Csf1*, and *Cxcr2*) were significantly up-regulated in TiO₂ NP-treated cells versus control cells (Figs. 3j and S5e). *Cxcr* (chemokine receptor) is expressed on myeloid cells, including neutrophils and monocytes [29]. Locally high levels of *Cxcl2* can recruit myeloid-derived suppressor cells. Furthermore, high levels of the calcium-binding small molecules *S100a9* and *S100a8* were produced by neutrophils (Fig. 3k). These molecules accelerated the migration of MDSCs to promote tumorigenesis or form premetastatic niches. Meanwhile, pathways associated with immunosuppression were activated in neutrophils [30] (Fig. 3l, m). In addition, non-immune stromal cells can also be affected by exposure to titanium materials. We observed fibroblasts around the TiO₂ NPs associated with an IL-17 immune response (Fig. 3m). These fibroblasts expressed high levels of the chemokines *Cxcl1*, *Cxcl5*, *Cxcl12* and *Cxcl14*, and the metalloprotein *Mmp-2* (Fig. 3n), indicating a protumour phenotypic state of fibroblasts.

Notably, T cells showed a high surface expression of T cell exhaustion markers, including *Pdcd1*, *Lag3*, *Ctla4*, *Klrg1*, *Ptger2*, and *Havcr2* (Fig. 3o). The proportion of exhausted T cells (PD-1⁺TIM-3⁺) was significantly increased in CD8⁺ T cells (Fig. S5b). Compared to untreated control, significant changes were observed in gene expression related to T cell activation, inflammatory response, Toll-like receptor signalling, NF- κ B signalling, and the IL-17 signal pathway (Fig. 3p, q). T cells from tissues surrounding the TiO₂ NPs presented a distinct transcriptomic profile from that of untreated tissue-resident macrophages and T cells. The TiO₂ NPs induced CD11b⁺ myeloid immune cells infiltration, which regulated T cell exhaustion and apoptosis in a cell-contact-dependent manner. Together, these results indicated that injection of TiO₂ NPs established an inflamed but immunosuppressive microenvironment by recruiting myeloid cells and altering the gene expression of myeloid cells to induce T cell exhaustion.

3.4. Implanted biomaterials promote local tumour growth in mice

We reasoned that tumour cells might grow efficiently in the tissue surrounding injected TiO₂ NPs due to the presence of CD11b⁺ myeloid cells and an immunosuppressive microenvironment. Healthy C57BL/6J mice were injected subcutaneously with TiO₂ NPs (day 0), and mice in the control group were injected with the same volume of phosphate-buffered saline (PBS). On the following day (day 1), B16F10-Luc melanoma cells were inoculated near the injection site. B16F10 melanoma cells grew significantly faster in TiO₂ NP-treated mice than in the control group based on bioluminescence imaging and tumour size assessment (Fig. 4a-c). On day 15, the average tumour weight of the TiO₂ NP group was ~3-fold that of the control group (Fig. 4d-f). The body weight of mice did not show a significant change over this roughly two-week period (Fig. 4g). PEGylation is widely used to modify biomaterial surfaces. We discovered that PEGylation of the TiO₂ NPs slowed the tumour growth caused by the unmodified TiO₂, but not to the rate of tumour growth observed in the untreated control group (Fig. S6). We tested several mouse tumour models; injection of the TiO₂ NPs accelerated tumour growth in subcutaneous MC38, CT26, and 4T1 carcinoma tumour models (Fig. 4h-j). These results indicated that the TiO₂ NPs could promote tumour growth around the injection site. Interestingly, in a B16 nude mouse tumour model in which the mice cannot

generate mature T lymphocytes, no significant difference was observed in tumour growth with or without TiO₂ NP injection (Fig. 4k). This result reinforced that TiO₂ NP treatment results in T cell dysfunction that contributes to tumorigenesis.

To broaden the scope of these findings, we examined the effects of other commonly used degradation-resistant biomaterial implants—single-wall carbon nanotubes, silicone gel, titanium alloy, and polyimide—on tumour growth at the implant site. We observed that mice injected with these biomaterials had significantly more significant tumour growth than untreated mice to varying degrees (Fig. 4l-o, Fig. S7).

Considering that TiO₂ NPs induced high PD-1 expression in recruited immune cells, we investigated the effect of a PD-1 blockade on tumour progression. Intravenous injection of anti-PD-1 antibody alone showed no effect on mice. Intriguingly, in mice injected with TiO₂ NPs, treatment with anti-PD-1 antibody resulted in a significant tumour growth delay and tumour burden reduction (Fig. S8a). We used flow cytometry to analyse the tumour-infiltrating immune cells on day 13. More CD3⁺ cells and CD8⁺ cells infiltrated tumours in TiO₂ NP-injected mice treated with anti-PD-1 than in the other groups (Fig. S8b and c). In addition, the proportion of cytotoxic T lymphocytes (CD3⁺CD4⁻CD8⁺) was significantly increased to ~30%, accompanied by a decrease in CD4⁺ T cells (Fig. S8d-f). CD8⁺ T cells showed elevated levels of Ki67⁺ (Fig. S8g and h), consistent with the anti-tumour effect. The ratio of CD8⁺ T cells to regulatory T cells (Tregs) increased ~2-fold compared to mice without the PD-1 blockade (Fig. S8i). Together, these results indicated that the PD-1 checkpoint blockade inhibited tumour growth effectively in TiO₂ NP-treated mice.

3.5. Vitamin C abolishes TiO₂ NP-induced immunosuppression and inhibits tumour growth in mice

Vitamin C (L-ascorbic acid, Vc) is an essential dietary nutrient important to a healthy immune system and can reduce inflammation and inhibit proinflammatory cytokine production [31, 32]. Previous reports have illustrated that vitamin C could effectively enhance the infiltration and functions of immune cells, such as T cells, macrophages, and dendritic cells [33,34]. We hypothesised that treatment with vitamin C might affect the immunosuppressive microenvironment established by implanted biomaterials. First, we studied the effects of vitamin C on TiO₂ NP-treated macrophages *in vitro*. RAW 264.7 cells were co-cultured with PBS (negative control), LPS (positive control), TiO₂ NPs, or TiO₂ NPs plus vitamin C for 24 h. Vitamin C significantly mitigated the increase in PD-1 expression caused by the TiO₂ NPs (Fig. 5a-c) by inhibiting the activation of the NF- κ B pathway (Fig. 5d). In addition, the levels of the inflammatory cytokines IL-6 and TNF- α decreased significantly (Fig. S9a, b).

To further investigate changes in the TiO₂ NP-induced immunosuppressive microenvironment by vitamin C, mice were injected with TiO₂ NPs and given a high dose (4 g/kg) of vitamin C intraperitoneally on days 0, 2, and 4. Tissues adjacent to the injection were removed for flow cytometry analysis. We discovered a marked reduction in the number of myeloid-derived suppressor cells (Fig. 5e) and PD-1⁺ immune cells (Fig. 5f-k), which were primarily T cells. The proportion of other detected immune cells did not change significantly. The ratio of PD-1⁺ T cells was considerably lower for treated versus untreated mice (25% versus 10%) (Fig. 5l, m). Both CD8⁺ T cells and CD4⁺ T cells showed lower PD-1 expression in treated mice (Fig. 5n, o). Vitamin C treatment restored T cell function as indicated by reduced expression of TIM-3 (Fig. 5p), LAG-3 (Fig. 5q) and CTLA-4 (Fig. 5r). Together, these results showed that vitamin C treatment reverses immune suppression in the microenvironment surrounding TiO₂ NP injection by restoring T cell function.

We investigated whether vitamin C treatment could alleviate the immunosuppressive effects generated by TiO₂ NPs. As observed previously, TiO₂ NP injection accelerated tumour growth compared to a control

group. Vitamin C treatment slowed the tumour growth rate based on the bioluminescence of tumour cells to a level similar to that in a blank control group (Fig. 5s, u). Similar results were observed in silicone gel-injected mice (Fig. S10). After analysing the infiltrating immune cells in the tumour, we found that Vc treatment promoted the infiltration of many CD3⁺ cells (Fig. 5v). The proportion of tumour infiltrating cytotoxic T cells doubled compared to the TiO₂ group, resulting in delayed tumour growth (Fig. 5w). Collectively, these results suggest that vitamin C treatment alleviates immunosuppression and inhibits tumour growth around the TiO₂ NPs.

4. Discussion and conclusion

The past decade has witnessed a rapid revolution in applying various implants in our lives, and some of them will change people's lifestyles in the future. For example, a brain chip implant shows promise to allow people whose spinal connections have been severed to restore movement. However, before the comprehensive application, a better understanding of the long-term biological effect of refractory-degradable implants *in vivo* is mandatory to ensure their efficacy and safety.

In this report, we discovered a phenomenon that foreign refractory-degradable biomaterial implants can establish an immunosuppressive microenvironment *via* recruitment of myeloid cells to induce T cell exhaustion, resulting in the promoted tumour growth at the injection site in mice tumour models. Our findings come from clinical patients who need bone replacement with titanium implants. To our surprise, although these titanium implants have been widely used in clinical for a long time, the tissues around the titanium plate were immersed in a large number of immune cells compared to normal tissue. These immune cells were most CD11b⁺ myeloid cells, including monocytes, macrophages, neutrophils and myeloid-lineage DCs. More importantly, we observed a significant increase in the PD-1 level of the myeloid cell and T cell populations.

To investigate the biological effect of refractory-degradable implants, TiO₂, which can be generated from titanium oxide layer on the titanium-based materials, was used as an example for in-depth study of the internal immune mechanism in mice. Single-cell RNA sequencing (scRNA-seq) was used to define how TiO₂ reshaped the injected site's immune landscape. Unlike normal tissues, the tissues nearby TiO₂ exhibited a microenvironment enriched in an immune suppression gene signature derived predominantly from myeloid populations. As a result, T cells were induced to produce dysfunction and exhaustion phenotype. Non-immune compartments, including fibroblasts, also contributed to the immunosuppressive microenvironment formation. These data demonstrate that the immunosuppressive microenvironment was established at the implant injection site, characterised by myeloid-rich, T cell-exhaustion gene signature. These factors compromised the ability of the immune system, particularly T cells, to respond to tumour cells at the local site.

Microenvironments influence tumour growth [30, 35–37]. Cancer cells do not survive in a normal immune microenvironment due to activated adaptive immunity and are killed by CD8⁺ cytotoxic T lymphocytes [38]. However, in an immunosuppressive microenvironment, T cells cannot control tumour growth [39]. Immunosuppressive environments, which promote immune evasion and support tumour growth [30, 40, 41], are associated with infiltration of immunosuppressive myeloid cells and the release of inflammatory cytokines, such as IL-10 and TGF- β [42], culminating in T cell dysfunction [43]. Similarly, the accumulation of bone-marrow-derived cells in the lung results in a premetastatic niche that promotes tumour metastasis [24]. Immunosuppressive myeloid cells promote the induction of regulatory T cells and elimination of effector T cells and have been linked with tumorigenesis [44–46]. We hypothesised that the immunosuppressive microenvironment would favour tumour growth. In subcutaneous MC38, CT26, and 4T1 carcinoma tumour models, we observed that tumour growth was increased at the TiO₂ NP injection site, but in a B16 nude mouse tu-

mour model in which the mice cannot generate mature T lymphocytes, no difference in tumour growth was observed. To broaden the scope of these findings, we examined several commonly used degradation-resistant biomaterial implants, including single-wall carbon nanotubes [47], silicone gel [48], titanium alloy [49] and polyimide [50], and discovered that promotion of tumour growth was independent of the type of implant material. These results indicate that foreign biomaterials establish a microenvironment that contributes to tumorigenesis.

Previous studies have reported that vitamin C treatment can effectively inhibit tumour growth by boosting the adaptive immune response in various cancer models [12]. In this study, we discovered that a high dose of vitamin C reduced PD-1 expression induced by implants. Administration of vitamin C rescued the immunosuppressive microenvironment surrounding foreign degradation-resistant implants and slowed tumour growth, providing a practical, low-cost approach to mitigate the carcinogenic nature of many biomedical materials. Other clinically approved antioxidants/anti-inflammatory agent supplementation in patients with implants should be future examined.

While our work suggests the link between the refractory-degradable implants and tumour growth, we did not observe neoplasia at the injection site during our experiments within one year—if we did not inject cancer cells, no tumour growth was observed. Our study was conducted using mouse tumour models, which do not accurately reproduce human cancer development; studies of longer-term effects of the implants are needed. Degradation and modification of implants are also likely to influence the establishment of an immunosuppressive microenvironment; for example, implant degradation may lead to the disappearance of immunosuppression. For long-term implants, surface modification may be essential to reduce myeloid cell accumulation. Lastly, although we discovered that Vc treatment could rescue the immunosuppressive microenvironment near foreign refractory-degradable implants, the dosages and treatment frequencies could be further studied and optimised. Nonetheless, this work suggests that refractory-degradable implants can establish a microenvironment *via* the recruitment of myeloid cells to induce T cell exhaustion, thus favouring tumour growth in multiple mice tumour models.

Declaration of interests

The authors declare that they have no conflicts of interest in this work.

Statistical analysis

Results are presented as mean \pm SEM. A two-tailed Student's *t*-test was used to calculate statistical differences between two groups; one-way ANOVA was used to compare more than two groups.

Acknowledgments

This work was supported by the National Natural Science Foundation of China (Grants No. 32022043, 81873995, 82102611), the Natural Science Foundation of Jiangsu Province (Grant No. SBK2019040088), the Jiangsu Province Six Talent Peaks Project (Grant No. SWYY-110), and the Social Development Key Programs of Jiangsu Province-Advanced Clinical Technology (Grant No. BE2019662). This work was also supported by the Program for Jiangsu Specially-Appointed Professors to C. W., and by the Collaborative Innovation Center of Suzhou Nano Science & Technology, the Priority Academic Program Development of Jiangsu Higher Education Institutions (PAPD), and the 111 Project.

Supplementary materials

Supplementary material associated with this article can be found, in the online version, at [doi:10.1016/j.fmre.2021.10.007](https://doi.org/10.1016/j.fmre.2021.10.007).

References

- [1] M.O. Dellacherie, B.R. Seo, D.J. Mooney, Macroscale biomaterials strategies for local immunomodulation, *Nat. Rev. Mater.* 4 (2019) 379–397.
- [2] A.K. Gaharwar, I. Singh, A. Khademhosseini, Engineered biomaterials for in situ tissue regeneration, *Nat. Rev. Mater.* 5 (2020) 686–705.
- [3] O.S. Fenton, K.N. Olafson, P.S. Pillai, et al., Advances in Biomaterials for Drug Delivery, *Adv. Mater.* 29 (2018) e1705328.
- [4] C. Wang, Y. Ye, Q. Hu, et al., Tailoring Biomaterials for Cancer Immunotherapy: Emerging Trends and Future Outlook, *Adv. Mater.* 29 (2017) 1606036.
- [5] L. Chung, D.R. Maestas Jr., A. Lebid, et al., Interleukin 17 and senescent cells regulate the foreign body response to synthetic material implants in mice and humans, *Sci. Transl. Med.* 12 (2020) eaax3799.
- [6] R. Trindade, T. Albrektsson, P. Tengvall, et al., Foreign Body Reaction to Biomaterials: On Mechanisms for Buildup and Breakdown of Osseointegration, *Clin. Implant Dent. Relat. Res.* 18 (2016) 192–203.
- [7] M.J. van Luyn, J.A. Plantinga, L.A. Brouwer, et al., Repetitive subcutaneous implantation of different types of (biodegradable) biomaterials alters the foreign body reaction, *Biomaterials* 22 (2001) 1385–1391.
- [8] J.M. Anderson, A. Rodriguez, D.T. Chang, Foreign body reaction to biomaterials, *Semin. Immunol.* 20 (2008) 86–100.
- [9] D.M. Higgins, R.J. Basaraba, A.C. Hohnbaum, et al., Localized immunosuppressive environment in the foreign body response to implanted biomaterials, *Am. J. Pathol.* 175 (2009) 161–170.
- [10] K.N. Ekdahl, J.D. Lambris, H. Elwing, et al., Innate immunity activation on biomaterial surfaces: A mechanistic model and coping strategies, *Adv. Drug Del. Rev.* 63 (2011) 1042–1050.
- [11] L. Tang, T.A. Jennings, J.W. Eaton, Mast cells mediate acute inflammatory responses to implanted biomaterials, *Proc Natl Acad Sci U S A* 95 (1998) 8841–8846.
- [12] A. Magri, G. Germano, A. Lorenzato, et al., High-dose vitamin C enhances cancer immunotherapy, *Sci. Transl. Med.* 12 (2020) eaax3799.
- [13] A.G. Bowie, L.A. O'Neill, Vitamin C inhibits NF-kappa B activation by TNF via the activation of p38 mitogen-activated protein kinase, *J. Immunol.* 165 (2000) 7180–7188.
- [14] S. Ferraris, A. Venturolo, M. Miola, et al., in: *Antibacterial and bioactive nanostructured titanium surfaces for bone integration*, 311, ApSS, 2014, pp. 279–291.
- [15] K.-L. Ou, Y.-H. Shih, C.-F. Huang, et al., in: *Preparation of bioactive amorphous-like titanium oxide layer on titanium by plasma oxidation treatment*, 255, ApSS, 2008, pp. 2046–2051.
- [16] R. Delgado-Ruiz, G. Romanos, Potential Causes of Titanium Particle and Ion Release in Implant Dentistry: A Systematic Review, *Int. J. Mol. Sci.* 19 (2018) 3585.
- [17] A. Mombelli, D. Hashim, N. Cionca, What is the impact of titanium particles and biocorrosion on implant survival and complications? A critical review, *Clin. Oral Implants Res.* 29 (18) (2018) 37–53 Suppl.
- [18] L. Yang, C.M. Edwards, G.R. Mundy, Gr-1+CD11b+ myeloid-derived suppressor cells: formidable partners in tumor metastasis, *J. Bone Miner. Res.* 25 (2010) 1701–1706.
- [19] Z. Zhang, S. Liu, B. Zhang, et al., T Cell Dysfunction and Exhaustion in Cancer, *Front. Cell Dev. Biol.* 8 (2020) 17.
- [20] E.J. Wherry, M. Kurachi, Molecular and cellular insights into T cell exhaustion, *Nat. Rev. Immunol.* 15 (2015) 486–499.
- [21] L. Bird, Myeloid PD1 in the frame, *Nat. Rev. Immunol.* 20 (2020) 72–73.
- [22] C. Blank, A. Mackensen, Contribution of the PD-L1/PD-1 pathway to T-cell exhaustion: an update on implications for chronic infections and tumor evasion, *Cancer Immunol. Immunother.* 56 (2007) 739–745.
- [23] A.P. Bally, P. Lu, Y. Tang, et al., NF-kappaB regulates PD-1 expression in macrophages, *J. Immunol.* 194 (2015) 4545–4554.
- [24] S. Kaczanowska, D.W. Beury, V. Gopalan, et al., Genetically engineered myeloid cells rebalance the core immune suppression program in metastasis, *Cell* 184 (2021) 2033–2052.
- [25] F. Lu, Y. Zhao, Y. Pang, et al., NLRP3 inflammasome upregulates PD-L1 expression and contributes to immune suppression in lymphoma, *Cancer Lett* 497 (2021) 178–189.
- [26] N. Ershaid, Y. Sharon, H. Doron, et al., NLRP3 inflammasome in fibroblasts links tissue damage with inflammation in breast cancer progression and metastasis, *Nat. Commun.* 10 (2019) 4375.
- [27] M. Moossavi, N. Parsamanesh, A. Bahrami, et al., Role of the NLRP3 inflammasome in cancer, *Mol. Cancer* 17 (2018) 158.
- [28] S.K. Wculek, I. Malanchi, Neutrophils support lung colonization of metastasis-initiating breast cancer cells, *Nature* 528 (2015) 413–417.
- [29] J. Hu, Q. Zhao, L.Y. Kong, et al., Regulation of tumor immune suppression and cancer cell survival by CXCL1/2 elevation in glioblastoma multiforme, *Sci Adv* 7 (2021) eabc2511.
- [30] D.F. Quail, J.A. Joyce, Microenvironmental regulation of tumor progression and metastasis, *Nat. Med.* 19 (2013) 1423–1437.
- [31] N. Mikirova, J. Casciari, A. Rogers, et al., Effect of high-dose intravenous vitamin C on inflammation in cancer patients, *J. Transl. Med.* 10 (2012) 189.
- [32] A.C. Carr, S. Maggini, Vitamin C and Immune Function, *Nutrients* 9 (2017) 1211.
- [33] R.A. Luchtel, T. Bhagat, K. Pradhan, et al., High-dose ascorbic acid synergizes with anti-PD1 in a lymphoma mouse model, *Proc Natl Acad Sci U S A* 117 (2020) 1666–1677.
- [34] N. Shenoy, E. Creagan, T. Witzig, et al., Ascorbic Acid in Cancer Treatment: Let the Phoenix Fly, *Cancer Cell* 34 (2018) 700–706.
- [35] K.E. de Visser, A. Eichten, L.M. Coussens, Paradoxical roles of the immune system during cancer development, *Nat. Rev. Cancer* 6 (2006) 24–37.
- [36] J.A. Joyce, J.W. Pollard, Microenvironmental regulation of metastasis, *Nat. Rev. Cancer* 9 (2009) 239–252.
- [37] M. Casanova-Acebes, E. Dalla, A.M. Leader, et al., Tissue-resident macrophages provide a pro-tumorigenic niche to early NSCLC cells, *Nature* 595 (2021) 578–584.
- [38] M.D. Vesely, M.H. Kershaw, R.D. Schreiber, et al., Natural innate and adaptive immunity to cancer, *Annu. Rev. Immunol.* 29 (2011) 235–271.
- [39] V. Kumar, S. Patel, E. Tcyganov, et al., The Nature of Myeloid-Derived Suppressor Cells in the Tumor Microenvironment, *Trends Immunol* 37 (2016) 208–220.
- [40] J.A. Joyce, J.W. Pollard, Microenvironmental regulation of metastasis, *Nat. Rev. Cancer* 9 (2009) 239–252.
- [41] T.F. Gajewski, H. Schreiber, Y.X. Fu, Innate and adaptive immune cells in the tumor microenvironment, *Nat. Immunol.* 14 (2013) 1014–1022.
- [42] M.A. Taylor, Y.H. Lee, W.P. Schiemann, Role of TGF-beta and the tumor microenvironment during mammary tumorigenesis, *Gene Expr* 15 (2011) 117–132.
- [43] M. Binnewies, E.W. Roberts, K. Kersten, et al., Understanding the tumor immune microenvironment (TIME) for effective therapy, *Nat. Med.* 24 (2018) 541–550.
- [44] S.M. Davidson, O. Jonas, M.A. Keibler, et al., Direct evidence for cancer-cell-autonomous extracellular protein catabolism in pancreatic tumors, *Nat. Med.* 23 (2017) 235–241.
- [45] M.-J. Park, S.-H. Lee, E.-K. Kim, et al., Interleukin-10 produced by myeloid-derived suppressor cells is critical for the induction of Tregs and attenuation of rheumatoid inflammation in mice, *Sci. Rep.* 8 (2018) 1–10.
- [46] J. Yu, M.D. Green, S. Li, et al., Liver metastasis restrains immunotherapy efficacy via macrophage-mediated T cell elimination, *Nat. Med.* 27 (2021) 152–164.
- [47] S.J. Teh, C.W. Lai, 5 - Carbon nanotubes for dental implants, in: A.M. Asiri, Inamuddin, A., Mohammad (Eds.) *Applications of Nanocomposite Materials in Dentistry*, Woodhead Publishing 2019, pp. 93–105.
- [48] M.H. Brown, R. Shenker, S.A. Silver, Cohesive Silicone Gel Breast Implants in Aesthetic and Reconstructive Breast Surgery, *Plast. Reconstr. Surg.* 116 (2005).
- [49] C.N. Elias, J.H.C. Lima, R. Valiev, et al., Biomedical applications of titanium and its alloys, *JOM* 60 (2008) 46–49.
- [50] S. Wurth, M. Capogrosso, S. Raspopovic, et al., Long-term usability and bio-integration of polyimide-based intra-neural stimulating electrodes, *Biomaterials* 122 (2017) 114–129.



Qin Fan received her Ph.D. degree from Soochow University in 2021, majored in chemistry. Since then, Dr. Qin Fan worked as a assistant professor at Nanjing University of Posts and Telecommunications, and focus on biomaterials and immunoengineering. Dr. Fan has published over 20 papers as first/corresponding author including *Science Advances*, *Matter*, *Advanced Functional Materials*, *Bioactive Materials*, *Theranostics*.



Chao Wang is a professor at Soochow University. He received his B.S. degree and Ph.D. degree from Soochow University. He has worked as a postdoctoral researcher at the University of North Carolina at Chapel Hill (UNC). In 2018, Dr. Wang joined FUNSOM at Soochow University as a professor. His research focuses on the construction of biomaterials for immunoengineering and immunotherapy for cancer, inflammation and auto-immunity. Dr. Wang has authored over 100 peer-reviewed papers, which have received a total citation of > 20,000 times and given him an H-index at 70. He was chosen for the 2018-2020 "Highly Cited Researchers" list produced by Clarivate Analytics.